Shock formation in a Q-device plasma

Michelsen, P.

Publication date:
1969

Document Version
Publisher's PDF, also known as Version of record

Risø Report No. 186

Risø Report No. 186

Danish Atomic Energy Commission

Research Establishment Risø

Shock Formation in a Q-Device Plasma

by Poul Michelsen

December, 1968

Sales distributors: Jul. Gjellerup, 87, Sölvgade, DK-1307 Copenhagen K, Denmark

Available on exchange from: Library, Danish Atomic Energy Commission, Risø, DK-4000 Roskilde, Denmark

Shock Formation in a Q-Device Plasma

by

Poul Michelsen

Danish Atomic Energy Commission
Research Establishment Risö
Physics Department

Abstract

Experiments on shock formation and shock reflection in a Q-device are described. In connection with these a numerical integration of the appropriate fluid equations is executed. The result of the experiments is that shock formation is possible when the ion temperature is decreased by ion-neutral collisions and the density is not too low. The shock reflection experiment indicates that $\gamma_{ion} = c_p/c_v = 5/2$. The numerically analysed fluid equations include the viscosity- and the heat-conduction terms, and also momentum and energy transfers between different kinds of particles are taken into account. Some stability and error-indication problems connected with the equations are considered.

CONTENTS

1. INTRODUCTION

During 1966 and at the beginning of 1967 a Q-machine [1,2] was designed and constructed by the Plasma Group at Risö with a view to basic research on a stationary alkali plasma. The first experiments performed with this machine were concentrated on propagation of shock waves and ion-acoustic waves through the plasma column generated in the machine. The main results of these experiments have been published [2-4]. Shock propagation in Q-machine plasmas has not been investigated earlier, while propagation of ion-acoustic waves has been examined in refs. 5 and 6. In the first of these works it is demonstrated that the propagation and damping of ion-acoustic waves may be explained by means of a theory in which the ions are treated on the basis of the linearized Vlasov equation and the electrons on the basis of the fluid equations.

The next step in this line of investigation is the study of the propagation of large density pulses which, under appropriate conditions, might be expected to develop into sharp fronts or "shocks". Experimental investigations of the properties of such propagation in connection with a numerical analysis of the problem on the basis of the fluid model are the subject of this report.

In section 2 we shall describe the experimental arrangement, importance being attached to those parts which are important for the understanding of the experiment. Section 3 presents the experimental results. These are concerned with the propagation of large density pulses through the plasma column, with the formation of shock fronts pertaining to this propagation, and finally with the reflection of the shock pulses.

In section 4 the fluid equations and the results obtained from the numerical calculations are discussed. These results are evaluated and compared with the experimental results in subsection 4.3. The method of numerical integration used is described in section 5. Section 6 presents the conclusion.

Many different people have participated in this work. Special thanks are due to Dr. N. D'Angelo, at whose suggestion the experimental work was initiated and under whose direction it was carried out, and to Professor O. Kofoed-Hansen for suggesting the numerical analysis.

This work was carried out in fulfilment of the requirements for obtaining the degree of lic. techn. at the Technical University of Denmark. The fellowship from that institution which made the study possible is gratefully acknowledged.

2. THE Q-MACHINE

The experiments were performed in the Q-device at the Research Establishment Risö. This device, which has been built at Risö, is quite similar in design to other alkali-plasma sources described in the literature. Therefore, only a brief informative description will be given here, with emphasis on the conditions decisive for the plasma state.

The principle of the Q-machine and the experimental arrangement is shown in fig. 1. The plasma is produced by surface ionization of alkali (Cs or K) atoms on a hot tantalum plate, about 2500°K. The neutral caesium is produced in an oven, from which, via a tube, it is guided against one of the tantalum plates. The caesium is produced by heating a mixture of CsCl and granulated Ca to about 400°C.

The plasma is radially confined by a homogeneous magnetic field of intensity up to 1 Wb/m^2, with an inhomogeneity of about 5%. The length of the plasma column may be varied, but normally has its maximum size 1.25 m. At the end opposite to the generating tantalum plate the column is terminated by a second plate. The temperature of this plate may also be varied up to about 2500°K. Both plates, which are 3 cm in diameter, are placed perpendicularly to the direction of the magnetic field. The tantalum plates are heated by electron bombardment from a filament mounted inside a separate vacuum system behind the tantalum plates. This arrangement makes it possible to allow a high neutral gas pressure in the main vacuum system, by means of which the percentage ionization may be varied without disturbance of the filament vacuum.

The pressure of the neutral gas in the main vacuum system may be varied from about $2 \cdot 10^{-6}$ torr upwards. This requires a few comments. At very low pressures ($\sim 2 \cdot 10^{-6}$ torr) the composition of the residual gas is unknown. At high pressures (above 10^{-2} torr) the plasma density will decrease quickly for two reasons: (1) the amount of neutral caesium striking the ionizing tantalum surface is reduced when the background pressure becomes so large that the mean free path of the caesium atoms becomes smaller than the distance from the oven tube to the tantalum plate, that is about 5 cm; (2) the neutral background gas will give rise to an enhanced diffusion of the plasma perpendicularly to the direction of the magnetic field.

Both the absolute density and its variation are measured solely with Langmuir probes of different sizes and shapes. Most of the data were ob-

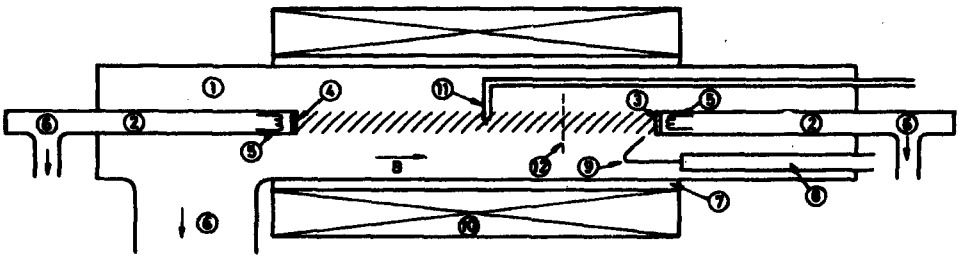

Fig. 1. Schematic outline of the Q-machine

1: Main vacuum vessel.
2: Cathode vacuum systems.
3: Generating cathode.
4: Reflecting cathode.
5: Filaments for electron bombardment of the cathodes.
6: To diffusion pumps.
7: Cooling jacket.
8: Caesium oven.
9: Caesium injection tube.
10: Magnetic field coils.
11: Langmuir probe.
12: Grid by means of which the plasma transmission can be varied.

tained with a cylindrical probe made of a tungsten wire. The probe was shielded from the plasma by a quartz tube so that only a tip 0.2 cm long and 0.02 cm in diameter was in connection with the plasma. By comparison with other diagnostic methods (e.g. microwaves), Langmuir probes of this size have been shown [7] to give the right absolute density within a factor of two when the density is greater than 10^{16} m^{-3}.

The introduction of a neutral gas in the vacuum system may be used to cool the ions. If a suitable amount of neutral particles is present, the ions will lose energy by collision and thereby be cooled [8]. The effect on the electron temperature T_e is considerably smaller because the cooling effect depends on the mass ratio of the colliding particles. The absolute density can be measured with a Langmuir probe on the assumption that the random-ion current to a negatively biased probe is given by

$$I = \frac{1}{4} qnv = \frac{1}{4} qn \sqrt{\frac{2 \varkappa T_i}{m_i}} ,$$

where q is the charge, n the ion density, v the ion thermal velocity, $\varkappa$ the Boltzmann constant, m_i the ion mass, and T_i the ion temperature. This expression would be valid if the presence of the probe caused no perturbation in the surrounding plasma. The probe does perturb the plasma, however. The ion current to the probe seems to be more a function of the electron temperature T_e than of the ion temperature [9]. This effect is due to the formation of a positive sheath round the probe, the size of which depends on the electron temperature. The electron temperature is rather constant and equal to that of the tantalum plates. For these reasons we may assume that the ion saturation current is directly proportional to the plasma density and independent of the ion temperature. This assumption has been used in measuring the data presented in this report.

Fig. 1 also shows a grid inserted in the plasma column, about 30 cm from the generating plate. The grid consists of parallel tungsten wires $2.5 \cdot 10^{-2}$ mm in diameter and spaced 0.3 mm. It is normally biased at -20 V with respect to the generating plate, which results in a plasma density distribution along the axis of the type shown in fig. 2. By a sudden change of the grid bias to approximately -2 V the grid is "opened", i.e., its transmission to the plasma is greatly enhanced. The "opening" of the grid in this arrangement is more or less equivalent to the breaking of the diaphragm in a conventional shock tube.

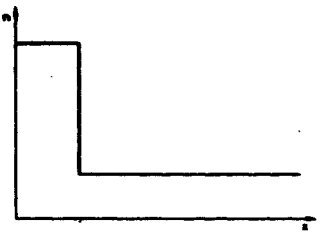

Fig. 2. Density distribution along the axis when the grid is "closed".

3. EXPERIMENTAL RESULTS

The experiments consisted in measuring the density as a function of time after producing a plasma pulse by a sudden "opening" of the grid. These measurements were made with Langmuir probes at several positions along the axis, i.e. the density n was measured versus x and t (position and time after the "opening" of the grid). The other essential parameters involved in the experiment are the initial plasma density and the neutral background pressure, which in a large region determines the ion temperature.

It is found convenient to divide the description of the results into two parts so that the measurements carried out with low and with high background pressure are treated separately.

Besides the measurements of the plasma pulse propagation, a connected experiment dealing with shock reflection is reported. The experimental arrangement for these measurements was quite identical with that described, but the arrival of the plasma pulse was measured both before and after its reflection on the hot tantalum plate.

3.1. Pulse Propagation at Low Pressure

The first series of measurements to be described were carried out in a plasma with a density in the region 10^{16} - 10^{18} m^{-3}, while the neutral pressure in all cases was below 10^{-5} torr. At such neutral pressure it is

normally assumed that $T_i = T_e = T_{pl}$ where T_{pl} is the temperature of the generating plate. From the kind of measurements mentioned, n versus x and t, the spreading of the pulse can be found. This spreading is shown in fig. 3 at different densities n_o and different density jumps $(n_2 - n_o)$; n_o is the density in front of the grid before the "opening", and n_2 is the somewhat higher density between the grid and the generating plate. By the term "spreading" we mean the increase of the pulse width w with x, where w in this connection is defined as

$$w \equiv \frac{n_2 - n_o}{(\frac{\partial n}{\partial t})_{max}} ,$$

i. e. the density jump divided by the maximum slope of the density versus the time curve at a certain position. The result of these measurements is

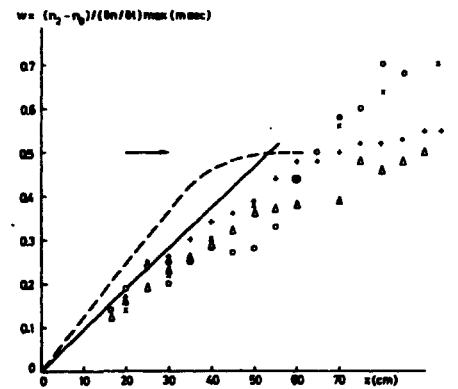

Fig. 3. Pulse width w vs. x for low neutral pressure ($p < 10^{-5}$ torr) and at several densities and pulse strengths [(x) $n_o = 2 \cdot 10^{10}$ cm^{-3}, $n_2/n_o = 4$; (+) $n_o = 4 \cdot 10^{10}$ cm^{-3}, $n_2/n_o = 5$; (o) $n_o = 1.2 \cdot 10^{11}$ cm^{-3}, $n_2/n_o = 2$; (Δ) $n_o = 3 \cdot 10^{11}$ cm^{-3}, $n_2/n_o = 5$;]. The dashed line is the pulse spreading computed from the fluid equations (at $n_o = 3 \cdot 10^{11}$ cm^{-3}, $n_2/n_o = 5$), and the solid line has been computed from the Landau damping model. The arrow shows the expected shock width ($n_o = 3 \cdot 10^{11}$, $n_2/n_o = 5$).

that the pulse width increases linearly with time, nearly independently of the density and the pulse strength, i.e. n_2/n_o. At great densities, 10^{18} m^{-3}, there is a tendency to shock formation when the pulse has moved more than about 60 cm. This is seen quantitatively by the deviation of the pulse width from the linear dependence on x, and qualitatively by the pulse front getting sharp edges.

3.2. Pulse Propagation at High Pressure

On an increase of the background pressure of the neutral gas it may be expected that the first thing to happen is a cooling of the ions because they lose some of their energy to the neutral particles by collision. The energy exchange between electrons and neutral particles is considerably smaller because of the mass ratio. If the background pressure is further increased, the momentum exchange between ions and neutrals may be expected to be important. This exchange is observed to damp the pulse considerably, but the measurements mentioned in the following were carried out in the pressure region where the cooling of the ions is expected to be dominant. The method of varying T_e/T_i with a neutral gas has been investigated in refs. 4 and 8.

In the present experiment the ion cooling was investigated by measuring the velocity of the pulse propagation as a function of the neutral gas pressure. This is shown in fig. 4 in two cases, Cs-ions cooled by He-atoms and by N_2-molecules. The plasma pulse begins to be delayed at some critical pressure $p \sim 1.5 \cdot 10^{-4}$ torr for N_2-cooling and $\sim 10^{-3}$ torr for He-cooling. The ratio between the two pressures is seen to be about equal to the mass ratio m_{He}/m_{N_2}, which indicates that we are observing ion-cooling. Fig. 4 shows, however, also another effect. The change of the pulse propagation velocity is greater than expected from ion cooling alone. As the velocity is proportional to $(\varkappa(T_i + T_e)/m)^{1/2}$, the variation should always be less than $\sqrt{2}$. This can be explained if we assume that at low gas pressures the plasma has a drift velocity from the generating to the reflecting plate. If this drift is decreased when the neutral pressure becomes sufficiently high, we obtain the effect mentioned.

When the pressure of the neutral gas is increased, the shape of the pulse front is changed into a sharp edge followed by a smooth rise up to the stationary level. This sharp leading edge must be interpreted as a shock front. In accordance with normal shock theory we define the shock

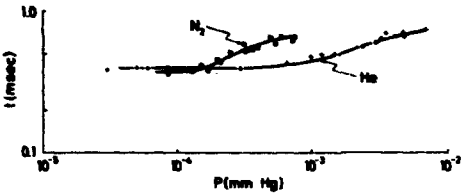

Fig. 4. The time, t, of arrival of the plasma pulse at x = 60 cm vs. the neutral gas pressure (He and N_2). $n \simeq 10^{12}$ cm^{-3}.

thickness as

$$w_s \equiv \frac{n_1 - n_o}{\left(\frac{\partial n}{\partial x}\right)_{max}} \qquad (1)$$

where n_1 and n_o are the densities behind and in front of the shock respectively, and $\left(\frac{\partial n}{\partial x}\right)_{max}$ is the maximum slope of the n versus x curve. In fig. 5

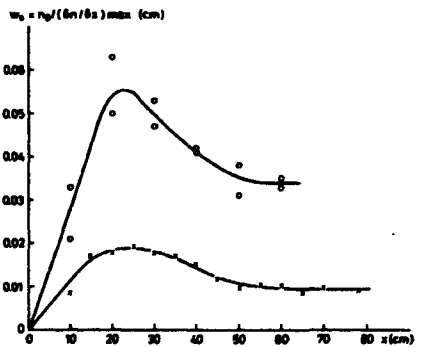

Fig. 5. Shock thickness w_s vs. x (x) density $n_o = 10^{12}$ cm^{-3}, neutral pressure (A) $p = 3 \cdot 10^{-6}$ torr, (o) $n_o = 1.5 \cdot 10^{11}$ cm^{-3}, $p(N_2) = 5 \cdot 10^{-6}$ torr.

the variation of w_s with x is shown. The thickness is seen to reach a stable value when x becomes sufficiently large.

The shock thickness as a function of the neutral pressure for different plasma densities and at a fixed position is shown in fig. 6. The thickness is in units of λ_o, the ion-ion mean free path at $T_i = T_e$, i.e. at the ion temperature at a low neutral pressure. The measuring points in fig. 6 represent cases where the pulse shape looks like a shock front, but they do not necessarily represent stable shock fronts. If we separate the pressure region into two parts, a low-pressure and a high-pressure region, we notice the following: At low pressures w_s/λ_o becomes constant in such a way that w_s seems to be independent of the density. This is in agreement with the curves in fig. 3 if we assume that the shock front has not reached its stable shape at the position x = 60 cm. At high pressures the curves at different densities coincide, which means that w_s/λ_o is only a function of p, the neutral pressure, and not of n, the plasma density. If we assume that the shock thickness is proportional to λ_{ii}, the mean free path of the

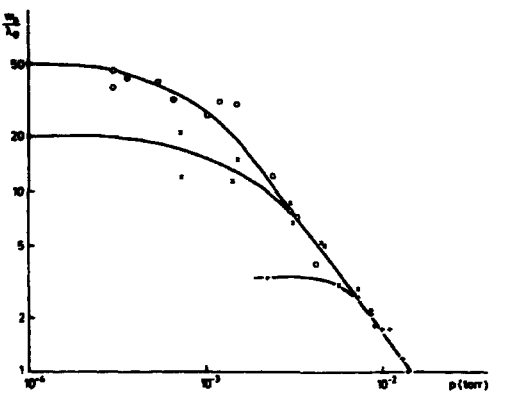

Fig. 6. Shock thickness divided by the ion-ion mean free path ($T_i = T_e$) w_s/λ_o vs. the neutral pressure (He), for x = 60 cm. [(o) $n_o = 5 \cdot 10^{11}$ cm^{-3}, $\lambda_o = 0.5$ cm, (x) $n_o = 1.5 \cdot 10^{11}$ cm^{-3}, $\lambda_o = 1.5$ cm, (+) $n_o = 3 \cdot 10^{10}$ cm^{-3}, $\lambda_o = 7.5$ cm].

ions at the actual temperature, it is seen that the cooling of the ions depends only on p. We shall later return to the meaning of this point.

The experimental results mentioned show that at low neutral pressures the pulse width increases linearly with time. On the other hand, at sufficiently high pressures the pulse takes on a certain shape, and its thickness remains constant. The latter effect is interpreted as the formation of a shock wave.

3.3. Shock Reflection

An important method of studying shock propagation is to examine the shock velocity versus the shock strength. Because of the previously mentioned unknown drift of the plasma column we cannot measure the shock velocity directly. If, however, we let the shock pulse be reflected on the hot plate opposite to the generating plate and assume that we have an ideal reflection, it is possible to eliminate the drift velocity. Further, such a shock reflection gives interesting information about the heating taking place when the shock pulse passes. We have investigated the dependence of the velocities of the generated and the reflected shock on the shock strength $S_I = n_1/n_o$, where n_1 and n_o are the densities behind and in front of the shock respectively. The results are shown in fig. 7. The times of arrival of the incident and of the reflected shock have been plotted as functions of the probe position x along the column, for different shock strengths. From that kind of curves the velocities have been measured and plotted as functions of the shock strength S_I. As expected, we see that the propagation velocity increases with increasing shock strength. These results will be discussed in the next section.

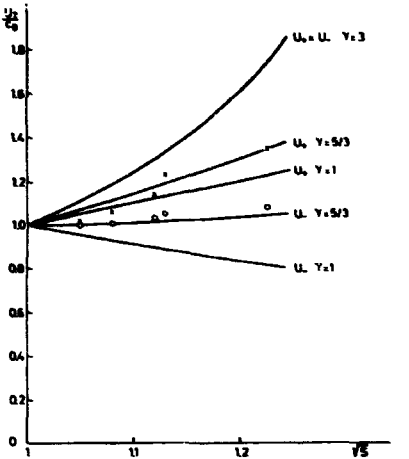

Fig. 7. Velocities of incident (x) and reflected (o) shocks vs. the square root of the shock strength. The solid lines are theoretical curves for different values of γ. U_+ and U_- are the velocities of the incident and the reflected shock respectively, calculated on the assumption $c_o = 1.2 \cdot 10^3$ m/sec and $v_D = 0.2\ c_o$.

4. THEORY AND DISCUSSION

To analyse the results presented in section 3 one may consider the behaviour of the plasma pulse on the basis of (a) the fluid equations, or (b) the Vlasov equation. The propagation of the plasma pulses may be expected to be closely connected with the propagation of ion-acoustic waves as investigated in refs. 4 and 5. The damping and the propagation velocity of these have been found in accordance with calculations on the basis of (b). The experiment described in ref. 6 shows that the Vlasov treatment fits satisfactorily when $\omega\tau_{ii} \rangle 1$, where ω is the frequency of the ion-acoustic waves and τ_{ii} is the ion-ion collision time. When $\omega\tau_{ii} \langle 1$, it is found that a fluid description gives a good representation of the experiment, which means

that the propagation velocity is decreased and that the damping mechanism is changed from Landau damping to viscous damping. From this we may conclude that the pulse propagation can be treated on the basis of (b) if $w_s/\lambda_{ii} \lesssim 1$, while the fluid equations will give a suitable description if $w_s/\lambda_{ii} \gg 1$. A discussion on the basis of the Vlasov equation will necessarily have to be of a qualitative nature as it is not possible to give a sufficient quantitative treatment of the non-linear phenomena we have examined. Nevertheless it might be expected that the propagation would be described suitably from the linearized Vlasov equation because the experiments show that the propagation is rather independent of the pulse strength within a large region ($1.2 < n_1/n_o < 5$). A result of this theory is that both the phase velocity and the ratio δ/λ between the damping length and the wave-length λ are constant. If we now Fourier-analyse our plasma pulse at the time of "opening" the grid and consider the propagation of each component, we find that the high-frequency components of the pulse die out over shorter distances than the low-frequency components. The net effect is, of course, a spreading of the pulse. If we define the pulse width as

$$w \equiv \frac{n_2 - n_o}{\left(\frac{\partial n}{\partial x}\right)_{max}} ,$$

we find, on the basis of the analysis mentioned, that this quantity grows linearly with time, in accordance with the experimental results in the case $T_i = T_e$. The propagation will of course also be independent of the density as the analysis is linear.

In the case of a reasonably great plasma density we would expect the fluid equations to describe the phenomena. At a density of $n = 5 \cdot 10^{17}$ m^{-3}, for instance, the ion-ion mean free path $\lambda_{ii} \simeq 5 \cdot 10^{-3}$ m, to be compared with the length of the machine $L = 1$ m. If the ions are cooled, the conditions for using the fluid equations are even better fulfilled because λ_{ii} is proportional to T_i^2.

In certain special cases it is possible to find a stationary solution to the fluid equations and in this way get some information about the shape of the shock front. In order to obtain some results about the propagation, the shape of the pulse before it becomes stable, and the time it takes the shock to build up, we carried out a numerical integration of the fluid equations. The actual numerical methods used are discussed in section 5. In 4.1 the equations used are discussed, in 4.2 the results of the numerical calcula-

tions are given, and in 4.3 they are compared with the experimental results. The reflected shocks are discussed in 4.4.

4.1. The Fluid Equations

Before we discuss the equations we have integrated, we shall consider a simpler case which can tell us a little about the shock front. We take a case where the pulse propagation is determined by the continuity and the momentum equation

$$\frac{\partial n}{\partial t} + \frac{\partial}{\partial x}(nu) = 0 \tag{2}$$

$$nm_i\left(\frac{\partial u}{\partial t} + u\frac{\partial u}{\partial x}\right) + \varkappa T_i \frac{\partial n}{\partial x} - \mu\frac{\partial^2 u}{\partial x^2} - nqE = P_{ie} + P_{in} \tag{3}$$

$$T_e\frac{\partial n}{\partial x} + nqE = P_{ei} = -P_{ie} \ . \tag{4}$$

As the plasma is quasi-neutral, the density n and the velocity u are the same for the ions and the electrons. We are concerned with propagation parallel to the direction of the B-field and may therefore ignore the presence of this field. In the momentum equation for the ions (3) we have introduced the following new quantities: m_i is the ion mass, q is the charge, $\varkappa$ is the Boltzmann constant, μ is the constant of viscosity of the ions, E is the electric field strength, P_{ie} is the total momentum transferred per unit time and unit length from electrons to ions because of collisions, and P_{in} is a similar quantity for the momentum transferred from the neutral particles. In the momentum equation for the electrons we have neglected the inertia terms and the electron viscosity which is allowed because the mass ratio $m_e/m_i \ll 1$. By substituting (4) in (3) we obtain the following equation for the momentum balance:

$$nm\left(\frac{\partial u}{\partial t} + \frac{\partial u}{\partial x}\right) + \varkappa(T_i + T_e)\frac{\partial n}{\partial x} - \mu\frac{\partial^2 u}{\partial x^2} = P_{in} \ . \tag{5}$$

Here we have made the assumption that both plasma components may be considered isothermal. This is very often done in calculations pertaining to Q-machine plasmas. As far as the electron gas is concerned, the argument for the assumption is that the heat conduction is sufficiently great to keep the electron temperature constant. For the ions the assumption can

sometimes be justified by the fact that the energy transfer between electrons and ions is sufficiently great to keep the temperatures equal. This does not seem to be the case here, as a simple calculation will show. A characteristic length in the experiment is the length of the plasma column: $L \simeq 1$ m. If we divide this by the phase velocity of an ion-acoustic wave, $c \simeq 10^3$ m/sec, we get an estimate of the total time a pulse needs to propagate through the whole machine:

$$\tau_p \simeq 1 \text{ msec.}$$

This is to be compared with the time at which equipartition of energy is established between ions and electrons (see e.g. ref. 10). At a density of $n = 10^{17}$ m^{-3} and a temperature $T = 2500^{\circ}$K the equipartition time is about

$$\tau_{eq} \simeq 4 \text{ msec}$$

and is inversely proportional to the density. Thus we see that $\tau_{eq} \gtrsim \tau_p$ in the experiment. On the other hand, the isothermal approximation makes the equations simpler, and most of the qualitative results will not be changed.

Let us for a moment make some additional simplifications of eqs. (2) and (5) by neglecting the viscosity term and the term for momentum transfer to the neutrals ($\mu = P_{in} = 0$). In this case the equations reduce to the type normally considered for the description of a simple fluid. One may therefore use all the considerations normally found in treatments of nonlinear behaviour of large-amplitude pulses in electrically neutral single fluids and obtain the conditions for shock formation. It is easy to deduce from such considerations[11] that were these simplified equations a complete representation of the plasma, shock production should occur. To get an idea of the width of the shock front we have to take the viscosity term into account. In this case it is possible to find a stationary solution to the equations of the form

$$f(n) = -\frac{m_i n_o c}{\mu M}(x - x_o) \,, \tag{6}$$

where

$$f(n) = \frac{1}{M^2} \ln \left(\frac{n}{n_o}\right) + \frac{1}{1-M^2} \ln \left(\frac{n}{n_o} - 1\right) + \frac{1}{M^2(1-M^2)} \ln \left(M^2 - \frac{n}{n_o}\right) \tag{7}$$

and

$$c = \left[\frac{\varkappa(T_i + T_e)}{m_i}\right]^{1/2}$$

is the phase velocity of an ion-acoustic wave, n_o is the density in front of the shock and M (Mach number) is the corresponding velocity divided by c. The expression (6) shows that the width of the shock front is inversely proportional to the density n_o or, in other words, directly proportional to the mean free path. From the definition of the shock width (1), and by using (6) and (7), we find

$$w_s \sim \frac{8\mu}{m_i n_o c} \frac{\sqrt{S}}{S^2-1} , \tag{8}$$

where $S = \frac{n_1}{n_o} = M^2$ is the shock strength. In accordance with ref. 10 we have for the ratio between the coefficient and the ion-ion mean free path

$$\frac{\mu}{\lambda_{ii}} = 1.76 \cdot m_i n_o \sqrt{\frac{\varkappa T_i}{m_i}} . \tag{9}$$

Using this in (8), we obtain the shock width in proportion to the mean free path:

$$\frac{w_s}{\lambda_{ii}} \simeq 14 \sqrt{\frac{T_i}{T_i + T_e}} \frac{\sqrt{S}}{S^2-1} .$$

In the experiment, $S \lesssim 1.5$, so in the case $T_i = T_e$ we have

$$w_s \gtrsim 10 \lambda_{ii} . \tag{10}$$

Let us now drop the isothermal approximation and take the temperature variations into account. It is a well-known fact that in the classic shock theory for neutral gases the heat conduction contributes to the width of the shock front an amount approximatively equal to that contributed by the viscosity effect. We may therefore expect the number in (10) to be in-

available at the Risö Computer Library, was used as the main part of the integration programme. This procedure is based on the Runga-Kutta method and has been improved by Merson[15]. The improvement makes it possible to calculate the expansion error, which is essential because it enables us to find the most convenient step length and thus to minimize the computation time. In order to increase the stability of the solutions, the smoothing operators mentioned in ref. 16 were used. They serve, essentially, as filters removing unwanted high-frequency oscillations caused by numerical instabilities.

The whole integration procedure is based on a mesh resulting from a division of the x- and t-axes into constant intervals of the lengths Δx and Δt respectively. The numerical differentiations were carried out by using "9-point operators" of the "central difference" type[16]. Different methods were used to obtain a survey of the accuracy of the calculations. It was attempted to keep the accumulated rounding-off errors and their propagation in order by including error equations. These rounding-off errors may be used for determining the step length Δt in the direction of the t-axis.

In the following we shall discuss the whole procedure in some detail.

The three equations to be integrated have been mentioned in the preceding section, but in a form that is not convenient for numerical calculation. By normalizing the quantities with respect to the density n_o, the velocity v_o and the temperature T_o, introducing the mean free path λ_o, and rearranging the terms, we give the equations the form

$$\frac{\partial n}{\partial t} = -n\frac{\partial u}{\partial x} - u\frac{\partial n}{\partial x} \tag{14}$$

$$\frac{\partial u}{\partial t} = -u\frac{\partial u}{\partial x} - \frac{\partial T_i}{\partial x} - ((T_e + T_i)\frac{\partial n}{\partial x} + \sqrt{T_i}(u \cdot \nu_{in} - \mu_o\lambda_o T_i \left(T_i \frac{\partial^2 u}{\partial x^2} + 2.5\frac{\partial T_i}{\partial x}\frac{\partial u}{\partial x}\right)))/n \tag{15}$$

$$\frac{\partial T_i}{\partial t} = -u\frac{\partial T_i}{\partial x} + (\gamma-1)(-T_i\frac{\partial u}{\partial x} + (T_i^{3/2}\lambda_o(\mu_o T\left(\frac{\partial u}{\partial x}\right)^2 + \eta_o(T_i\frac{\partial^2 T_i}{\partial x^2} + 2.5\left(\frac{\partial T_i}{\partial x}\right)^2))))/n) - \nu_{ei}(T_i - T_e)_n - (T_i - T_n)\nu_{in}/n . \tag{16}$$

The only quantities not yet defined are T_n, the temperature of the neutrals, and ν_{ei}, the electron-ion collision frequency.

In writing the dependence on n, u and T_i explicitly, we may consider the quantities ν_{ei}, ν_{in}, μ_o, and η_o as constants.

The system of equations (14) - (16) now has the form

$$\frac{\partial v_i}{\partial t} = f_i\left(v_j, \frac{\partial v_j}{\partial x}, \frac{\partial^2 v_j}{\partial x^2}\right) = F_i(v_j) \quad , \tag{17}$$

where the v's represent the density, velocity and temperature. In principle we may now find the solution by using a Taylor expansion. Assuming that v is known at the time t_o, in all the positions x_r ($0 < r \leq N$), we see that $v(t_o + \Delta t, x_r)$ is given by

$$v(t_o + \Delta t, x_r) = \sum_{n=0}^{p} \frac{(\Delta t)^n}{n!} \frac{\partial^n v}{\partial t^n}(t_o, x_r) + R \quad , \tag{18}$$

where R is the remainder term, which gives the expansion error if we ignore it. The derivatives in (18) can be found from (17), for instance:

$$\frac{\partial^2 v_i}{\partial t^2} = \frac{\partial f}{\partial t} \cdot \left(\frac{\partial v_j}{\partial t}, \frac{\partial}{\partial x}\left(\frac{\partial v_j}{\partial t}\right), \frac{\partial^2}{\partial x^2}\left(\frac{\partial v_j}{\partial t}\right)\right) \quad . \tag{19}$$

The higher-order derivatives can always be expressed in a form similar to (19), where the right-hand side only contains the first derivative of v with respect to t; it may be inserted from (17), and the derivatives with respect to x may be found by numerical differentiation. However, the higher-order derivatives found from (19) become rather complicated and make the Taylor method troublesome. The principle of other integration procedures is not essentially different, but instead of the derivatives being calculated as in (19) only the first derivative is used, and the new values of v are found by an iteration method or by calculating v in some intermediate points between t_o and $t_o + \Delta t$.

The Runga-Kutta method is a fourth-order process, i. e. it is identical with a truncated Taylor expansion up to and including the fourth derivative. Instead of calculating the four derivatives one calculates the first derivative in four points, the extreme points (t_o and $t_o + \Delta t$) and two intermediate

points. In the Runga-Kutta method improved by Merson, which we have used, the first derivative is calculated in five points instead of four. This makes it possible to find an approximate expression for the expansion error, which may be used for determining the step length Δt in the direction of the t-axis. This step length may then be chosen so that the expansion term becomes smaller than a fixed limit.

The equations (14) - (16) are of the parabolic type, and therefore, in order to determine v if $t > t_o$, it is not sufficient to know $v(t_o)$ in a certain x-interval. To get a complete fixing of the particular solutions we must assume that v is known on the border $x = x_o$ and $x = x_1$ for all $t \geq t_o$. The derivatives of v with respect to x have to be calculated by means of some numerical approximation method. We have used the differential operators as introduced in ref. 16. For our purpose we just replace the n^{th} derivative by

$$\frac{\partial^n v}{\partial x^n}(t, x_r) = \frac{1}{(\Delta x)^n} \sum_{s=-h}^{h} \frac{C_r^{(p,n)}}{C^{(p,n)}} v(t, x_r + s\Delta x) \quad , \tag{20}$$

where s is an integer summation index and $C_r^{(p,n)}$ and $C^{(p,n)}$ are integer coefficients and denominators given in the above-mentioned reference. $p = 2h + 1$ is an odd integer defining the number of points around x_r used for calculating the derivative. The expression (20) corresponds to the derivative to be found in the point x_r by fitting a polynomium of maximum degree 2h to the values of v in the points $x = x_r + s\Delta x$. The value of v at the time $t + \Delta t$ is found from the equations

$$v_1 = v_o + 1/3\, \Delta t\, f(t, v_o)$$

$$v_2 = v_o + 1/6\, \Delta t\, [f(t, v_o) + f(t + \Delta t/3, v_1)]$$

$$v_3 = v_o + 1/8\, \Delta t\, f(t, v_o) + 3/8\, \Delta t\, f(t + \Delta t/3, v_2)$$

$$v^1(t+\Delta t) = v_4 = v_o + 1/2\, \Delta t\, f(t, v_o) - 3/2\, \Delta t\, f(t+\Delta t/3, v_2) + 2\, \Delta t\, f(t+\Delta t/2, v_3)$$

$$v(t+\Delta t) = v_5 = v_o + 1/6\, \Delta t\, f(t, v_o) + 2/3\, \Delta t\, f(t+\Delta t/2, v_3) + 1/6\, \Delta t\, f(t+\Delta t, v_4) \; ;$$

v_0 is the value of v at the time t; v_1, v_2, ... v_5 and v^1 are some auxiliary variables, and the function f(t, v) is the derivative as indicated in (17). If the interval Δt is sufficiently small, f(t, v) may be represented by the linear approximation

$$f(t, v) = At + Bv + C .$$

In this case it can be shown that the error of v_4 is $-1/120(\Delta t)^5 \partial^5 v/\partial t^5$ and that of v_5 is $-1/720(\Delta t)^5 \partial^5 v/\partial t^5$. We may then assume that a good estimate of the error of v_5 is $1/5(v_4 - v_5)$. If a maximum permissible error is chosen in advance, the step length can easily be found when it is taken into account that the error varies as the step length to the fifth power.

For parabolic differential equations of the non-linear type the problems about convergence and stability are rather complicated. The first of these is actually unsolved, while the concept of stability has to be replaced by local stability, assuming that the function varies slowly across small regions. As the stability depends on the solution, which of course is unknown in advance, it is difficult to say anything in general about it. The problems in connection with equations similar to ours have been investigated analytically in ref. 17, but we have chosen to use the numerical method mentioned in ref. 16.

Supposing that v has been encumbered with a small error e ($e \ll v$), we can introduce it into (17), which yields

$$\frac{\partial e_i}{\partial t} = F_i(v_j + e_j) - F_i(v_j) + S , \qquad (21)$$

where S is a source term arising for instance from rounding-off errors. Equation (21) is similar to (17) and the calculations of the errors can be carried out side by side with these equations. As we have assumed e to be small, we may linearize (21). The stability may be examined by finding the effect of introducing a small e (and S = 0). If we obtain an exponential growth, the method of solution is unstable, which will be the case when $\Delta t/(\Delta x)^n$ becomes too large; n means the highest order occurring of the space derivatives. Again, this maximum allowable ratio $\Delta t/(\Delta x)^n$ depends on the solution and cannot be found generally. On the other hand one wants to use a Δt as large as possible in order to save computation time. In the integration method used, Δt has been determined on the basis of knowledge of the expansion error, which implies security against instability. If the

ratio $\Delta t/(\Delta x)^n$ becomes larger than a certain value, the solutions will be unstable, and the estimated expansion error will grow very quickly, exceeding the allowable size. This causes the calculation to start again from the previous integration step, with the new value of Δt:

$$\Delta t_{new} = \Delta t \left(\frac{\delta}{\epsilon}\right)^{1/5} \cdot K \ , \qquad (22)$$

where δ is the allowable value of the expansion error, ϵ is the actual value, and K is a constant a little smaller than one.

The method of error estimation by means of eq. (21) has the advantage that it can be used to minimize the total error. Assume that the source term S can be found as a good representation of the rounding-off errors which will be introduced in each integration step. Then the error equation (21) will give the total accumulated rounding-off error at a certain time, and it will be possible to choose a step length such that the expansion error can be neglected in comparison. The source term S may be found from a knowledge of the rounding-off method used in the actual computer or by the method discussed in ref. 16. The calculations we performed, including equation (21), all showed linear error growth, the total accumulated errors never exceeding the permissible limit. This observation was also made in another way. If two calculations are performed with different step lengths, for instance differing by a factor of two, we may expect the expansion errors to differ by a factor of 2^5 and the rounding-off errors by a factor of 2. If the step length is decreased, the expansion error will also decrease, while the rounding-off error will increase, and vice versa. The difference between two such calculations indicates the size of the errors involved. In an actual case the relative difference was found to be below 10^{-5}. In the above considerations it has been assumed that the step length was in all cases below the necessary limit for stability.

Until now we have only concentrated on the step length in the t-direction, Δt. Also the finite step length in the x-direction will cause errors, corresponding to the difference approximation introduced in expression (20).

An estimate of this finite x-step error can be obtained by a method similar to that mentioned above, by changing the value of the x-step length. Results from such calculations show that if we do not have a large change in v (equation 17) over less than five steps in the x-direction, the error will not exceed 1%. Here we must remark that we have approximated the derivatives by 9-point differentiation operators, corresponding to p = 9 in expres-

sion (20).

In connection with numerical calculations that may give rise to discontinuities, as for instance shock fronts, there will always be problems with the step length in the x-direction. If the dissipative terms are neglected in problems of our kind, the exact solution contains a discontinuity. In ref. 17 this problem is solved by introducing a "pseudo-viscosity", which smoothes out the shock front. The conditions on both sides of the shock are shown to be unchanged, as is the shock velocity, while the shape of the shock front is of course changed. In our calculations we have dissipative terms in the equations, so the width of the shock front will always have a finite value. The shock width is unknown in advance, but in order to optimate the calculation (that is to find the best compromise between accuracy and computing time), it is suitable to fix the step length from a knowledge of the maximum slope contained in the solution. This can be done just by an estimate of the slope or by carrying out a Fourier analysis of the solution at suitable intervals.

The stability of the equations is improved by using the smoothing operators introduced in ref. (16). This prevents the most unstable oscillation (wave length $\lambda = 2\ \Delta x$) from growing and at the same time damps the other high frequencies. Thus it is possible to increase the t-step length Δt without making the solutions unstable.

6. CONCLUSION

The result of section 3 demonstrates that it is possible to make shock propagation parallel to the B-lines in a Q-machine when the density is high and the ion temperature sufficiently low. It seems that these shocks may be appropriately described by the fluid equations when they have been formed. Because of our uncertain knowledge of many of the parameters involved in the problem it is difficult to obtain much more than qualitative agreement with theory, and only a few quantitative comparisons between experiment and calculations have been carried out.

The shock width and velocity are found to be in good accordance with theory, and also the variation of the shock width with the ion temperature can be explained from the fluid equations. The experiment with shock reflections indicates that the best agreement between experiment and fluid model is obtained if we choose γ_{ion} equal to 5/3. The propagation of plas-

creased by a factor of 2. Together with the two equations (2) and (5) we shall now consider the equation for conservation of energy [11,12]:

$$n\frac{k}{\gamma-1}\left(\frac{\partial T_i}{\partial t}+u\frac{\partial T_i}{\partial x}\right)+n k T_i\frac{\partial u}{\partial x}-\mu\left(\frac{\partial u}{\partial x}\right)^2-\frac{\partial}{\partial x}\left(\eta\frac{\partial T_i}{\partial x}\right)=\left(\frac{\partial E}{\partial t}\right)_{coll}, \tag{11}$$

where γ is the ratio of the specific heat at constant pressure to that at constant volume, and η is the constant of heat conduction [13]. The physical meaning of each term in (11) from left to right is as follows: the rate of change of thermal energy of an element of the fluid per unit volume, the work done in changing the size of the element, the work done because of viscous forces, the heat flowing into the element because of thermal conduction, and (the term on the right-hand side of the equation) the rate of change of the thermal energy of the element due to collisions with particles of other kinds (electrons and neutrals). The last-mentioned term may be written as

$$\left(\frac{\partial E}{\partial t}\right)_{coll}=n k\frac{T-T_i}{\tau_{eq}},$$

where T is the temperature of the other particles and τ_{eq} the corresponding equipartition time. τ_{eq} for electrons is given in ref. 10, while for neutrals we have

$$\tau_{eq}\simeq\frac{1}{\nu_{in}}\frac{m_i}{m_n}\qquad(m_i\gg m_n),$$

where ν_{in} is the ion-neutral collision frequency, and m_i/m_n is the mass ratio between ions and neutrals. If in eqs. (5) and (11) we neglect the dissipative terms and the terms that account for the momentum and energy transfer to other kinds of particles, we may again use the normal shock theory. According to the latter, a function specifying the density, which is a step function at $t = 0$, will at $t > 0$ be split into three characteristic regions connected by constant levels as shown in fig. 8. Foremost is the shock front propagating with the shock velocity. Then comes a contact surface, which is a discontinuity in density and temperature moving with the surrounding fluid. At the back we see the rarefaction wave moving backward with the acoustic velocity and spreading out linearly with time. The

different density levels and the corresponding velocities and temperatures may be found from the shock conditions, which are determined by the conservation equations integrated over a discontinuity. If we do not neglect any terms in the equations, we cannot calculate analytically how the density pulse will propagate. It will of course be split up into the same three regions, and the levels will be equal after some time. The shock front may be expected to reach a stable shape, while the rarefaction wave and the contact surface will gradually spread out.

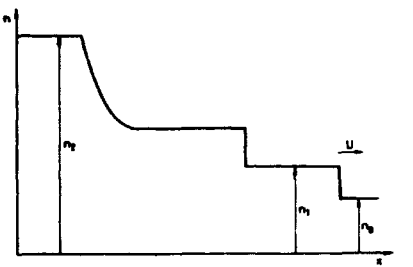

Fig. 8. Shock propagation when the dissipative terms are neglected.

4.2. Numerical Results

The results of the numerical calculations may be divided into three parts, (1) the propagation of the density pulse as a function of the shock strength when $\nu_{in} = 0$; (2) the effect of the neutral gas on the pulse propagation, and (3) the importance of the initial values of the drift velocities. Typical results for the pulse propagation are shown in the appendix. From such curves the shock width w_s may be obtained. The reciprocal of this quantity times the mean free path λ_o/w_s versus the shock strength S is shown in fig. 9. For small values of S the curve is identical with other results given in the literature (e.g. ref. 14), which are calculated for cases where the dissipative terms have a different temperature dependence. The curve shows that λ_o/w_s has a maximum for $S \simeq 2$, which is due to the marked temperature dependence of the viscosity - and the heat conduction term. When the shock strength increases, the temperature vari-

ation across the shock front also increases, which means that the mean free path and with that the shock thickness will be larger. In this connection we have to remember that the equations can only be expected to be valid if the shock strength is not too great.

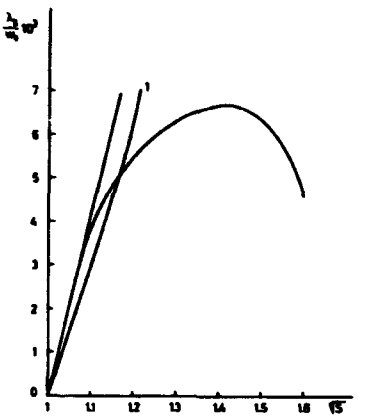

Fig. 8. Calculated curves of the ion-ion mean free path divided by the shock thickness vs. the square root of the shock strength. 1: the isothermal case; 2: the dissipative terms independent of temperature (μ = constant); 3: the dissipative terms proportional to $T^{5/2}$ ($\mu \propto T^{5/2}$).

A quantity of interest for a comparison with the experiment is the time it takes the shock to become stable. It is questionable, however, whether the fluid equations can give a good answer because the propagation starts with a density distribution that varies much over a distance comparable to the mean free path. We must, however, expect the pulse to spread out at the beginning with a velocity near the ion-acoustic velocity, which is in agreement with the result we obtain from the fluid equations. This result is shown together with the experimental points in fig. 3. Under the reasonable assumption that the plasma drift velocity is about half the ion-acoustic velocity, it fits satisfactorily.

The calculations also show the formation and propagation of the contact surface and the rarefaction wave. These will not be further discussed because they cannot be compared with the experimental work.

The next series of calculations were executed with different values of the ion-neutral collision frequency and unchanged initial conditions. One difficulty here is to determine a relation between the background pressure and the ion temperature. The calculations were made on the assumption that the ion temperature would be determined by the balance resulting from the fact that the energy the ions lose by collisions with the neutral particles is equal to the energy they receive by collisions with the electrons. The characteristic time τ_{eq} necessary for this balance to be established is $\simeq 1/\nu_{in}\, m_i/m_n$, the equipartition time for ions in a neutral gas. If the lifetime of the ions τ_L is short compared with τ_{eq}, which is the case if the drift of the column is large, the ion temperature only depends on the pressure of the neutral gas p and not on the density n, but varies through the column. In the opposite case the temperature also depends on the plasma density. In figs. A3-A5 in the appendix the propagation of the plasma pulse is shown as it changes when the ion-neutral collision frequency is increased. When T_i is decreased, we see as expected that the shock width is decreased until the amount of neutral particles is so large that the plasma pulse starts losing momentum. When this happens, the pulse is spread out quickly. According to the calculations the minimum shock thickness is obtained when the ratio of the ion-ion mean free path to the ion-neutral mean free path is

$$\frac{\lambda_{ii}}{\lambda_{in}} \simeq 10^{-3} \ ,$$

which will give a cooling of the ions by about a factor of 4. If the ratio $\lambda_{ii}/\lambda_{in}$ becomes larger, the damping caused by momentum loss begins to be of importance.

A very large part of the ions in the experiment recombine on the grid before "opening". This means that the plasma will have different drift velocities on the two sides of the grid. Such a situation is shown in fig. A6, where the initial drift velocity is $\simeq 0.3$ c towards the centre, that is, the difference between the drift velocities on the two sides is $\simeq 0.6$ c, where c is the ion-acoustic velocity. The result is, as shown, that the shock strength is increased while the size of the rarefaction wave is decreased.

4.3. Comparison with Experimental Results

The experiments carried out at a low background pressure show that the pulse width increases linearly with time, and only at very high plasma densities is there a tendency to shock formation. As shown in fig. 3, the time needed to establish a stable shock front, as calculated from the fluid equations, is comparable to the time it takes the pulse to move through the full column, especially if we assume the plasma drift velocity to be about equal to the ion thermal velocity. In section 4 it is mentioned that a velocity of pulse spreading may be found from a Fourier analysis on the basis of Landau damping. This is also shown in fig. 3. The result is seen to be close to that calculated on the basis of the fluid equations.

According to fig. 8 the shock width itself cannot be less than about $15\,\lambda_0$ and, in a certain region, is $(1.3 < S < 2)$ rather independently of the shock strength. In this region most of the experiments were carried out.

At high pressures we find experimentally a clear shock formation, as appears for instance from fig. 5. The fact that the front length first increases and then decreases is not expressed by the fluid equations, but may be due to the fact that the ions are cooled more and more as they move down through the column. This must be the case if the ion-neutral collision frequency is high compared with the ion lifetime; then the ion temperature is simply determined by the number of collisions with neutral cold particles suffered by the ion. This is in agreement with fig. 6, which shows that w_s/λ_0 does not depend on the plasma density when the shock has reached its stable width. The curve in fig. 6 is in qualitative agreement with the fluid consideration concerning the decrease of w_s/λ_0 with decreasing ion temperature. On the basis of the previously mentioned difficulty of finding the connection between T_i and ν_{in} it is not possible to draw qualitative parallels to the numerical calculations.

4.4. Reflected Shocks

The results of the experiments with reflected shocks mentioned in section 3 are illustrated in fig. 7. The figure shows the velocities of the incident shock U_+ and the reflected shock U_- versus the shock strength S. To describe these propagation phenomena we may use the shock equations[11], and for the velocities we easily find

$$U_+ = c \sqrt{\frac{S(1-\mu^2)}{1-\mu^2 S}} \tag{12}$$

$$U_- = U_+ \frac{\mu^2(2-S)-1}{S(1-\mu^2)} \quad , \tag{13}$$

where c is the ion-acoustic velocity and

$$\mu^2 = \frac{\gamma-1}{\gamma+1} \quad .$$

These equations are valid for a normal gas-dynamic shock in a polytropic gas, but in the fluid approximation they also describe the shock propagation for the plasma with $\gamma = \gamma_{ion}$, as the electrons only influence c. Fig. 7 shows theoretical curves calculated on the basis of the above equations (12) and (13) with different values of γ. The experimental points are plotted on the assumption that the drift velocity was

$$v_D = 0.2\ c$$

and

$$c = 1.2 \cdot 10^3 \text{ m/sec.}$$

From these results we get the best fit to the theoretical curves if we choose $\gamma_{ion} = 5/3$. Especially U_- shows good agreement with the theoretical curve. The measurements are encumbered with a rather large uncertainty, as also appears from their variance.

5. INTEGRATION OF THE FLUID EQUATIONS

The equations discussed in subsection 4.1 were solved by numerical integration on the IBM 7094 computer at NEUCC.

This computation work was carried a little further than was necessary just to make comparisons with the experiments. The purpose of this was to study the interesting stability problems arising in connection with the solution of this kind of problems, and to work out a general integration procedure that might be used for similar problems.

A standard procedure for solving n simultaneous differential equations,

ma pulses narrower than or about equal to the ion-ion mean free path is also examined. The width of these is found to increase linearly with time, independently of density and pulse strength.

We may expect the Vlasov equation to be appropriate in this case.

In section 5 we have discussed a method of numerical integration of the fluid equations. Especially, we have mentioned some stability problems and possibilities of error indication.

REFERENCES

1) N. Rynn and N. D'Angelo, Device for Generating a Low Temperature, Highly Ionized Cesium Plasma. Rev. Sci. Instr. 31, 1326-1333 (1960).

2) H.K. Andersen, N. D'Angelo, P. Michelsen, and P. Nielsen, Experiments on Shock Formation in a Q-Device. Phys. Fluids 11, 606-610 (1968).

3) H.K. Andersen, N. D'Angelo, P. Michelsen, and P. Nielsen, Investigation of Landau-Damping Effects on Shock Formation. Phys. Rev. Lett. 19, 149-151 (1967).

4) H.K. Andersen, N. D'Angelo, V.O. Jensen, P. Michelsen, and P. Nielsen, Effects of Ion-Atom Collisions on the Propagation and Damping of Ion-Acoustic Waves. Phys. Fluids 11, 1177-1180 (1968).

5) A.Y. Wong, R.W. Motley, and N. D'Angelo, Landau Damping of Ion Acoustic Waves in Highly Ionized Plasmas. Phys. Rev. 133, A436-A442 (1964).

6) R.W. Motley and A.Y. Wong, in: P. Hubert and E. Cremien (editors), Proceedings of the Sixth International Conference on Ionization Phenomena in Gases (Bureau des Editions, Centre d'Etudes Nucléaires de Saclay, Paris, 1964) Vol. III, 133.

7) N. D'Angelo and S.V. Goeler, Plasma Losses in a Q-Device. Phys. Fluids 5, 279 (1965).

8) F.P. Blau, E. Guilino, M. Hashmi, and N. D'Angelo, Ion-Cooling in a Q-Device. Phys. Fluids 10, 1116-1117 (1967).

9) C.B. Wharton, Plasma Probing, Risö Report No. 18, 613 (1960).

10) Lyman Spitzer, Jr., Physics of Fully Ionized Gases (Interscience Publishers, New York - London, 1962).

11) R. Courant and K.O. Friedrichs, Supersonic Flow and Shock Waves (Interscience Publishers, New York, 1948).

12) W. Marshall, Kinetic Theory of an Ionized Gas. AERE T/R 2247 (Harwell, 1960).

13) W. Marshall, Kinetic Theory of an Ionized Gas, Part 2. AERE T/R 2352 (Harwell, 1960).

14) C. T. Chang, A Review of Shock Wave Theories. Risø-M-504 (1967).

15) G. N. Lance, Numerical Methods for High Speed Computers (Iliffe, London, 1960).

16) O. Kofoed-Hansen, Error Indicators for the Numerical Solution of Non-Linear Wave Equations. Risö Report No. 177 (1968).

17) J. Von Neumann and R. D. Richtmeyer, A Method for the Numerical Calculation of Hydrodynamic Shocks. J. Appl. Phys. 21, 232 (1950).

APPENDIX

The following calculated curves show the propagation of a sharp pulse. The density vs. x has been drawn at different values of t. The unit in the x-direction is the ion-ion mean free path λ_o (at $T_i = T_e$) in front of the shock. The unit in the t-direction is λ_o/u_o, where u_o is a characteristic velocity $u_o = (\varkappa T_o/m)$. Figures A3-A5 have been calculated with different amounts of neutral gas present, characterized by the ratio λ_o/λ_{in}, where λ_{in} is the ion-neutral mean free path. The curves at t = 0 show the initial value of the density. For the velocity we have u = 0 at t = 0 except in fig. A6, where $u(x < 0) = \frac{1}{2} u_o$ and $u(x > 0) = -\frac{1}{2} u_o$. In figs. A1, A2 and A6 there are no neutral particles and the initial value of the temperature is $T_i = T_e$ = constant. In the remaining figures the ratio T_e/T_i at t = 0 is given below the curve.

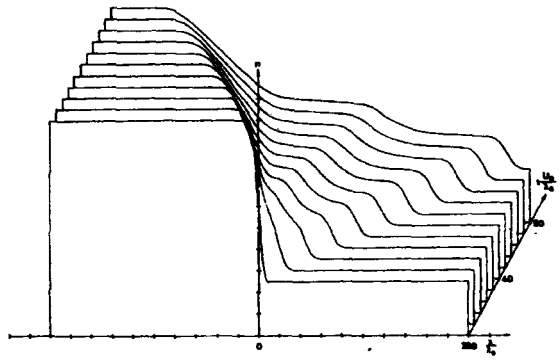

Fig. A1. $\lambda_{11}/\lambda_{12} = 0$.

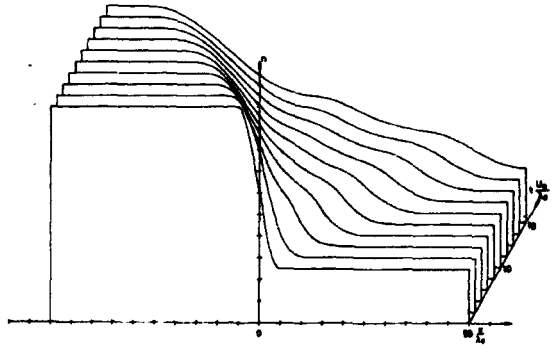

Fig. A2. As A1, but in another scale.

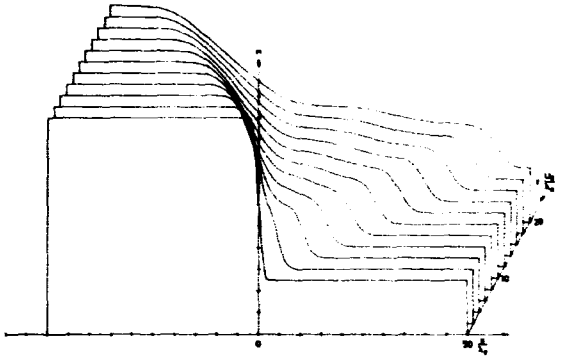

Fig. A3. With neutral gas pressure. $\lambda_{ii}/\lambda_{in} = 1.7 \cdot 10^{-4}$. $T_e/T_i(x < 0) = 1.05$, $T_e/T_i(x > 0) = 1.7$.

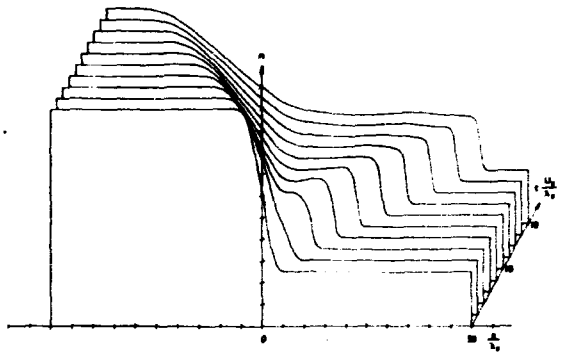

Fig. A4. $\lambda_{ii}/\lambda_{in} = 10^{-3}$. $T_e/T_i(x < 0) = 1.5$, $T_e/T_i(x > 0) = 4.9$.

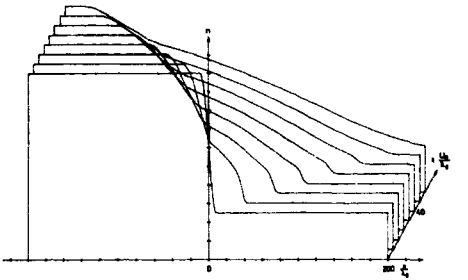

Fig. A5. $\lambda_{ii}/\lambda_{in} = 8 \cdot 10^{-3}$. $T_e/T_i(x < 0) = 7$. $T_e/T_i(x > 0) = 7.9$.

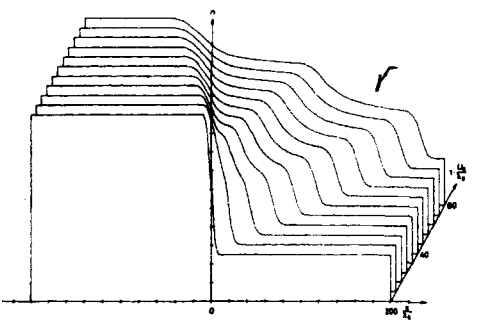

Fig. A6. $\lambda_{ii}/\lambda_{in} = 0$. $u(x < 0) = \frac{1}{2} u_o$, $u(x > 0) = -\frac{1}{2} u_o$.